RSC Advances

PAPER

View Article Online
View Journal | View Issue

Cite this: *RSC Adv.*, 2023, **13**, 10667

Cu(II) immobilized on poly(guanidine-sulfonamide)-functionalized Bentonite@$MgFe_2O_4$: a novel magnetic nanocatalyst for the synthesis of 1,4-dihydropyrano[2,3-*c*]pyrazole†

Sedigheh Alavinia, Ramin Ghorbani-Vaghei,* Ramin Ghiai and Alireza Gharehkhani

Received 4th January 2023
Accepted 20th March 2023

DOI: 10.1039/d3ra00049d

rsc.li/rsc-advances

In this paper, we aim at synthesizing a new nanocomposite material in which bentonite acts as a nucleation site for $MgFe_2O_4$ nanoparticles precipitation in the attendance of an external magnetic field ($MgFe_2O_4$@Bentonite). Moreover, poly(guanidine-sulfonamide), as a novel kind of polysulfonamide, was immobilized on the surface of the prepared support ($MgFe_2O_4$@Bentonite@PGSA). Finally, an efficient and environment-friendly catalyst (containing nontoxic polysulfonamide, copper, and $MgFe_2O_4$@Bentonite) was prepared by anchoring a copper ion on the surface of $MgFe_2O_4$@Bentonite@PGSAMNPs. The synergic effect of $MgFe_2O_4$ magnetic nanoparticles (MNPs), bentonite, PGSA, and copper species was observed while conducting the control reactions. The synthesized Bentonite@$MgFe_2O_4$@PGSA/Cu, which was characterized using energy-dispersive X-ray spectroscopy (EDAX), scanning electron microscopy (SEM), transmission electron microscopy (TEM), thermogravimetric analysis (TGA), X-ray diffraction (XRD), and Fourier-transform infrared (FT-IR) spectroscopy, was applied as a highly efficient heterogeneous catalyst to synthesize 1,4-dihydropyrano [2,3-*c*] pyrazole yielding up to 98% at 10 minutes. Excessive yield, quick reaction time, using water solvent, turning waste to wealth, and recyclability are the important advantages of the present work.

1 Introduction

Multicomponent reactions (MCRs), in which three or more compounds are combined together to prepare a product, are a straightforward and atom-economic synthetic approach that suggests notable advantages over conventional multistep reaction sequences.[1–3] In these protocols, the whole range of compounds could be synthesized by minimizing waste, time, and cost without intermediate isolation.[4–6] Mostly, MCRs exhibit several advantages such as speed, simple workup, environment friendliness, short reaction times, higher yields, use of non-toxic solvents, and no use of column chromatography for purification.[7–10] In recent years, many publications based on MCRs have been reported, which emphasizes their highlighted applications in organic and medicinal chemistry.[11–14]

1,4-Dihydropyrano[2,3-*c*]pyrazole is a specific heterocyclic pharmacophore with diverse medicinal chemistry and several interesting pharmacological and therapeutic characteristics.[15–18] Moreover, it is used as the core moiety to prepare many well-known drugs having antifungal, anti-inflammatory, antitumor, and several other pharmaceutical and bioorganic features (Fig. 1).

Recently, several catalytic systems have been developed to enhance the reaction conditions. Notably, each technique involves specific advantages and opens a new horizon in synthesizing 1,4-dihydropyrano[2,3-*c*] pyrazole[18–25] (Scheme 1). Nevertheless, such catalytic systems have shortcomings such as long reaction time, tedious workup, difficult reusability and recovery of precious metal catalysts, and environmental hazards.

Regarding the growing interest of organic chemists in nanocomposites, several studies have been conducted on these materials due to the unique surface and physical properties of these heterogeneous catalysts in different organic reactions.[26–31] Nowadays, magnetic nanoparticles, which are one of the most influential factors in the nanomaterial family, have been extensively employed in different sciences, consisting of drug shipping, sickness recognition, water desalination, and chemical catalysis.[3,31] Among magnetic nanoparticles, nanophase spinel ferrites with superparamagnetic behavior are presently utilized in drug transport, microwave devices, catalytic activity, and magnetic imaging.[4,32–35] As valuable materials, ferrites are compounds with different and useful physical properties along with high chemical stability and low production cost.[36] Among diverse structures, spinel ferrites are the most important class

Department of Organic Chemistry, Faculty of Chemistry, Bu-Ali Sina University, Hamedan, 6517838683, Iran. E-mail: rgvaghei@yahoo.com; ghorbani@basu.ac.ir; Fax: +98 81 38380647

† Electronic supplementary information (ESI) available. See DOI: https://doi.org/10.1039/d3ra00049d

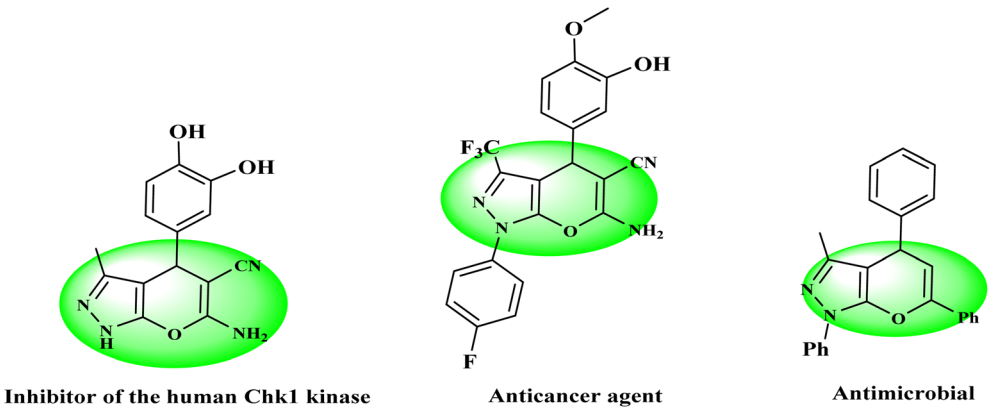

Fig. 1 Selective examples of pharmaceutically important 1,4-dihydropyrano[2,3-*c*]pyrazole.

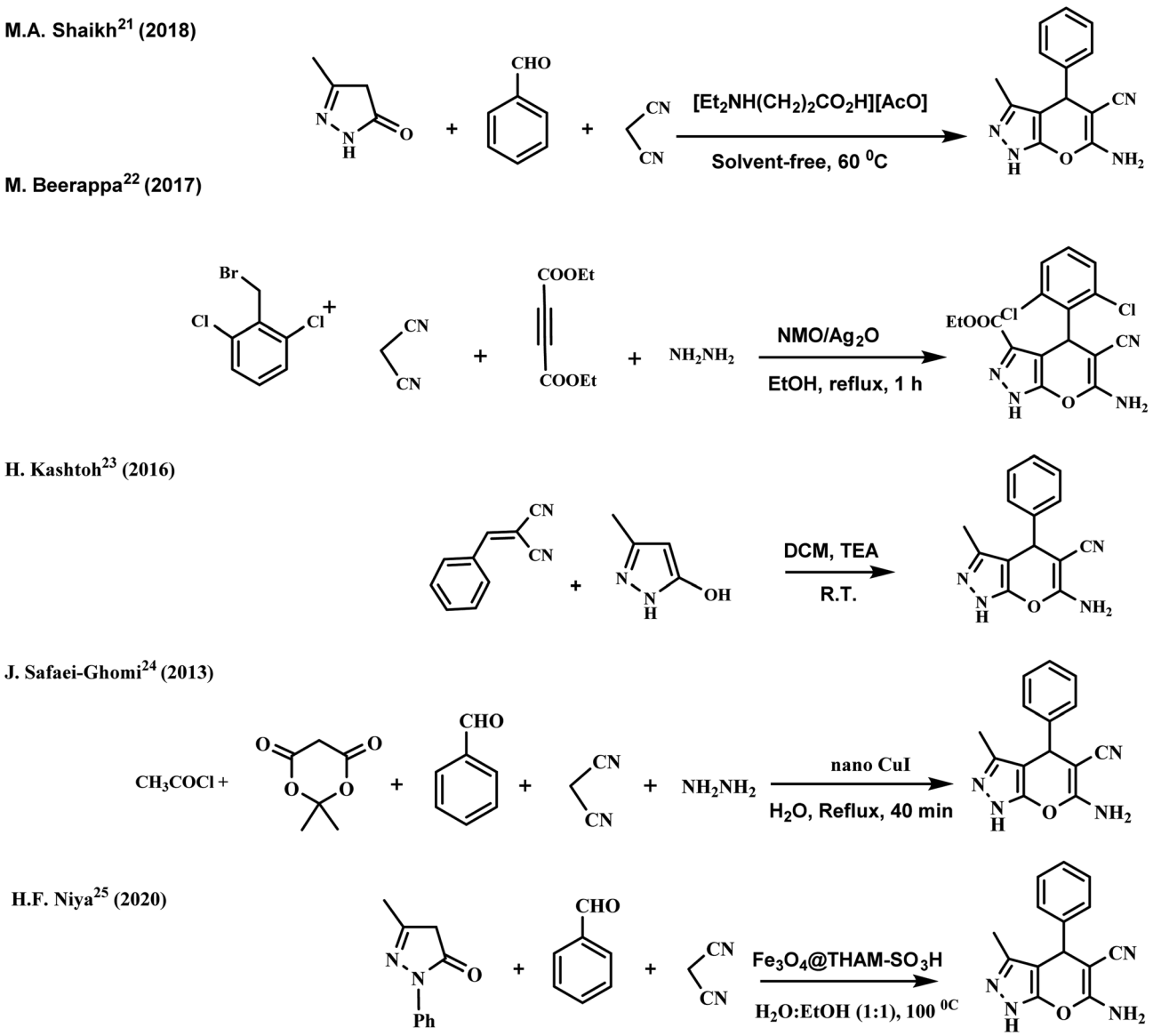

Scheme 1 Recent methods for the synthesis of 1,4-dihydropyrano[2,3-*c*] pyrazole.

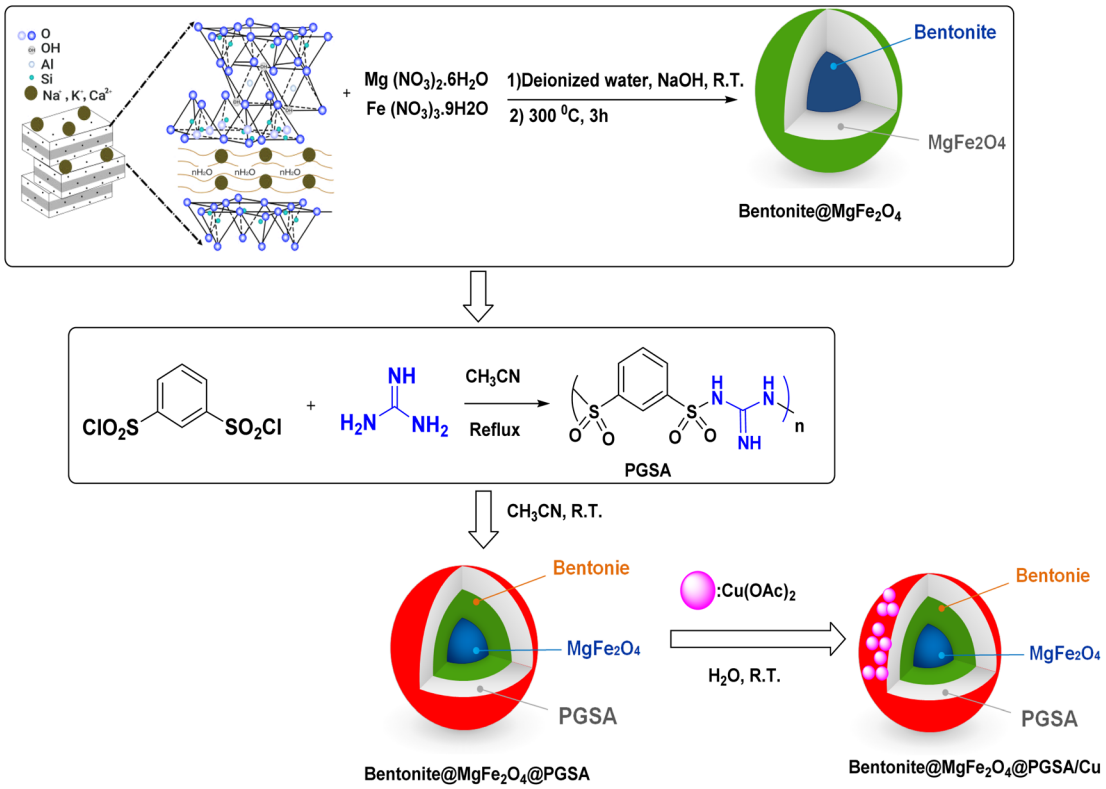

Fig. 2 Schematic representation of the synthesized Bentonite@$MgFe_2O_4$@PGSA/Cu nanocomposite.

and are divided into normal and inverse forms, in which Mg/Fe_2O_4 has great applicability owing to its potential for use in different fields.[37,38] In this regard, the functionalization of ferrite-based nanocomposites is a useful method to improve the physicochemical features and compatibility. Ferrite magnetic nanoparticles can be functionalized with organic and inorganic compounds such as rice husk, ash, chitosan, activated carbon, and clay materials to synthesize nanocomposites based on ferrites.[29,39–41]

Clay materials, such as quartz, talc, calcite, and dolomite, have three-dimensional porous frameworks, tunable surface functionalities, large surface area, and pore channels with regular geometry.[40–42] Because of their inherent advantages, clays have been widely used in constructing biomedicine, chemical sensing, heterogeneous catalysts, and dye adsorption.[43] Therefore, synthesizing magnetic clay to develop atom-economic reactions and reduce negative environmental impact can be a useful process.

In this regard, magnetic clay is a promising inorganic compound incorporated in a polymer matrix to synthesize a polymer/clay nanocomposite.[28,44] However, this system offers low compatibility between the polymer and clay, leading to a defective structure and irregular morphology. In this respect, the choice of the polymer and clay matrix pair is very important in polymer/clay construction regarding its role in their performance and morphology.

Polysulfonamides are among the other highly-interesting compounds used in medicinal chemistry and to prepare heterogeneous catalysis.[45] Polysulfonamides have good chemical stability, great surface area, and low skeleton density.[45–47] The final structure of the polysulfonamides was controlled by the appropriate selection of the monomers. In this sense, guanidine has been used to prepare a novel organic polymer support (PGSA) (Fig. 2).

Herein, regarding the abovementioned points and following our current efforts in exploring green catalytic protocols toward chemical synthesis, a new organometallic nanocatalyst is synthesized, which consists of magnetic bentonite and PGSA and offers the advantages of both materials. Furthermore, the problem of separation was directly solved in a sense that the number of active sites having nanomagnetic features increased. Copper ions were then successfully decorated on the prepared support (Bentonite@$MgFe_2O_4$@PGSA/Cu) (Fig. 2). Eventually, the nanocatalyst was successfully incorporated in a three-component reaction to prepare the new pyrano[2,3-*c*]pyrazoles. This pharmaceutically valuable nanocatalyst was fabricated through mild reaction conditions using H_2O with short reaction times (Scheme 2). Notably, this study is the first report on the catalytic application of Bentonite@$MgFe_2O_4$ @PGSA/Cu MNPs.

2 Experimental

2.1. Chemicals and instruments

All the chemicals, reagents, and equipment used in this study are listed in Table 1.

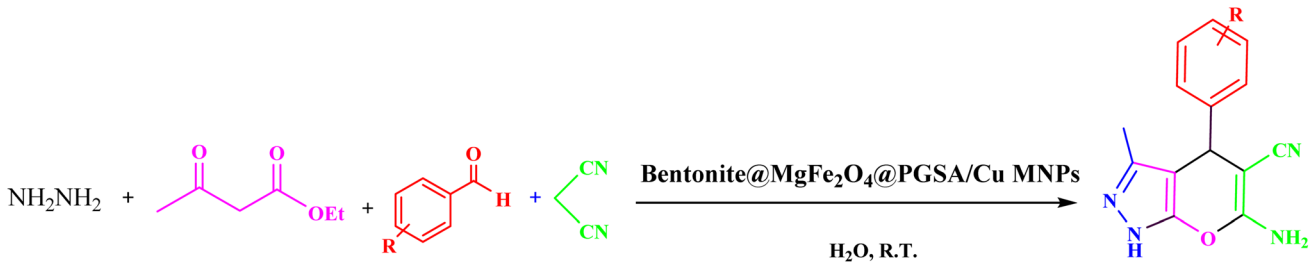

Scheme 2 Synthesis of 1,4-dihydropyrano[2,3-*c*]pyrazole derivatives using Bentonite@$MgFe_2O_4$@PGSA/Cu nanocomposite.

Table 1 Chemicals and equipment used in this study

Materials and equipment	Purity and brand
Bentonite stone	Sigma Aldrich (≥99.995%)
Guanidine	Sigma Aldrich (99.9%)
$FeCl_2 \cdot 4H_2O$	Sigma Aldrich (98%)
$FeCl_3 \cdot 6H_2O$	Sigma Aldrich (≥98%)
K_2CO_3	Merck (98%)
Sodium hydroxide	Merck (97%)
Ethanol	Sigma Aldrich (97%)
Acetonitrile	Merck (98%)
Sodium borohydride	Sigma Aldrich (≥96%)
FT-IR analysis	Shimadzu IR-470 spectrometer
EDX analysis	Numerix DXP-X10P
SEM analysis	Sigma-Zeiss microscope
TEM analysis	Philips Cm 12 instrument
XRD analysis	JEOL JDX-8030 (30 kV, 20 mA)
NMR analysis	Varian Unity Inova 500 MHz
Ultrasound cleaning bath	KQ-250 DE (40 kHz, 250 W)
Melting point measurement	Electrothermal 9100, made in UK

2.2. Preparation of Bentonite@$MgFe_2O_4$ NCs

$MgFe_2O_4$–bentonite nanoparticles were prepared through a hydrothermal method using 8.7 mmol ferric nitrate, 8.7 mmol magnesium nitrate, and bentonite (1 g) in an aqueous solution pH 12 (adding sodium hydroxide (1 M)), which was then stirred for 1 h. Afterward, black nanoparticles were separated using an external magnet, washed with distilled water and dried at 80 °C overnight. The prepared catalyst was calcined in a muffle furnace at 300 °C for 3 h (Fig. 2).

2.3. General procedure for the synthesis of poly(guanidine-sulfonamide) (PGSA)

Benzene-1,3-disulfonyl chloride (10 mmol) was added to 5 mL acetonitrile, and then, guanidine (20 mmol in 5 mL CH_3CN) was added dropwise to the initial mixture and stirred under reflux condition for about 6 h (Fig. 2).

2.4. Bentonite@$MgFe_2O_4$@PGSA/Cu synthesis

The functionalization of Bentonite@$MgFe_2O_4$ was done *via* PGSA coating on the surface of Bentonite@$MgFe_2O_4$. In this regard, 1.0 g PGSA was dispersed in 100 mL acetonitrile, which was followed by the addition of Bentonite@$MgFe_2O_4$ (1.0 g). Besides, it was at room temperature that the reaction mixture was stirred for 4 h. Afterward, the resulting mixture was filtered out and washed with acetonitrile (10 mL). Subsequently, the synthesized support (1.0 g) was dispersed in 50 mL H_2O using an ultrasonic bath (15 min). Thereupon, 0.5 g $Cu(OAc)_2$ was dissolved in 5 mL H_2O and then it was added to the previous mixture. After stirring the mixture for 5 h, the resulting precipitate was separated and washed with 50 mL H_2O and, finally, it was dried in an oven (Fig. 2).

2.5. General procedure for the synthesis of substituted 1,4-dihydropyrano[2,3-*c*]pyrazole derivatives

Benzaldehyde (1 mmol), malononitrile (1 mmol), ethyl acetoacetate (1 mmool), hydrazine hydrate (1 mmol), and Bentonite@$MgFe_2O_4$@PGSA/Cu (10 mg, 0.2 mol%) were stirred in water solvent at room temperature. After the completion of the reaction (monitored by TLC), Bentonite@$MgFe_2O_4$@PGSA/Cu catalyst was isolated by an external magnet, washed with EtOH and EtOAc (2 × 5 mL), and dried under vacuum. The title compounds were obtained in their crystalline forms by the recrystallization of ethanol solution (Scheme 1).

3 Results and discussion

3.1. Characterization of Bentonite@$MgFe_2O_4$@PGSA/Cu nanocomposite

Fig. 3 illustrates the Fourier transform infrared (FT-IR) spectra of PGSA, Bentonite@$MgFe_2O_4$, Bentonite@$MgFe_2O_4$@PGSA,

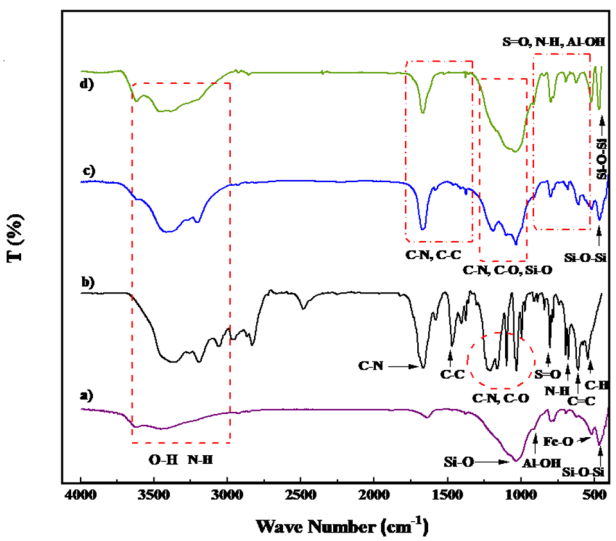

Fig. 3 FT-IR spectra of (a) Bentonite@$MgFe_2O_4$, (b) PGSA, (c) $MgFe_2O_4$@Bentonite@PGSA, (d) $MgFe_2O_4$@Bentonite@PGSA/Cu.

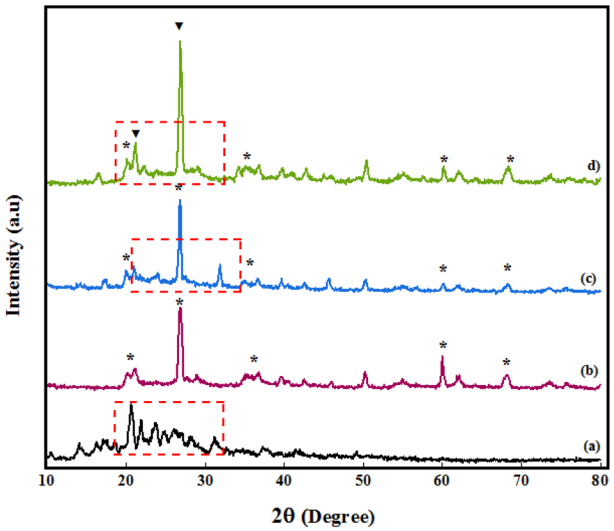

Fig. 4 XRD spectrum of (a) PGSA, (b) Bentonite@$MgFe_2O_4$, (c) Bentonite@$MgFe_2O_4$@PGSA, (d) Bentonite@$MgFe_2O_4$@PGSA/Cu.

and Bentonite@$MgFe_2O_4$@PGSA/Cu nanocomposite. Regarding the Bentonite@$MgFe_2O_4$ spectrum, the absorption bands at 471, 520, 780, 926, and 1055 cm^{-1} belong to the tensile vibrations of the Si–O–Si, Fe–O, Mg–O, Al–OH, and Si–O bonds, respectively (Fig. 3a). Considering the FT-IR spectrum of PGSA, the broad band at 3200–3700 cm^{-1} indicates the presence of NH and NH_2. The vibration bands at 1338 and 1160 cm^{-1} (because of the O=S=O stretching) demonstrate the presence of sulfone bridges in the PGSA. Furthermore, the absorption bands at 1664 and 1682 cm^{-1} indicate the presence of guanidine (Fig. 3b). According to the spectral information of Bentonite@$MgFe_2O_4$ and PGSA, it was observed that in the Bentonite@$MgFe_2O_4$@-PGSA spectrum (Fig. 3c), all tensile vibrations of PGSA and Bentonite@$MgFe_2O_4$ have appeared. Finally, regarding the Bentonite@$MgFe_2O_4$@PGSA/Cu nanocomposite spectrum (Fig. 3d), the interaction between the support and Cu shifted the C–N vibration to about 1675 cm^{-1} (1685–1675 cm^{-1}). The results from the comparison of the FT-IR spectra propose that

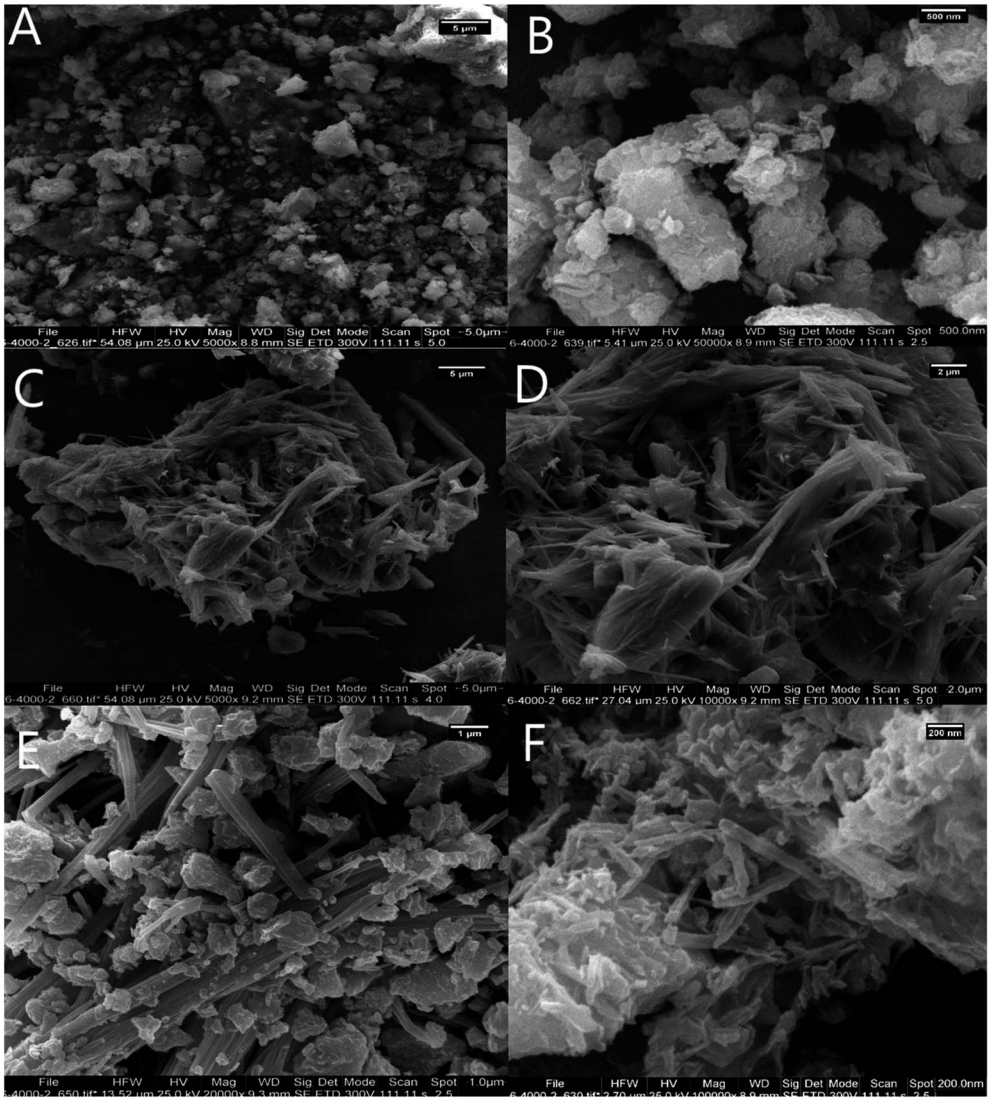

Fig. 5 FESEM image of (A and B) Bentonite, (C and D) PGSA, (E) Bentonite@$MgFe_2O_4$@PGSA, (F) Bentonite@$MgFe_2O_4$@PGSA/Cu.

PGSA and copper have been successfully loaded on the surface of Bentonite@$MgFe_2O_4$.

Structural identification of PGSA, Bentonite@$MgFe_2O_4$, Bentonite@$MgFe_2O_4$@PGSA, and Bentonite@$MgFe_2O_4$@PGSA/Cu nanocomposite systems was also carried out using XRD analysis (Fig. 4). Considering the XRD pattern of PGSA, the diffraction peaks at 2θ = 27.8°, 29.72°, and 30.67° are related to the triazine, guanidine, and sulfonamide groups, respectively, and have good crystalline properties (Fig. 4a). Regarding the XRD pattern of Bentonite@$MgFe_2O_4$, the diffraction peaks at 2θ = 23° and 28° can be attributed to bentonite, and the peaks at 61° and 69° belong to $MgFe_2O_4$. Moreover, Fig. 4c shows the XRD pattern of Bentonite@$MgFe_2O_4$@PGSA. The observed peaks indicate PGSA layers around Bentonite@$MgFe_2O_4$, confirming the formation of the Bentonite@$MgFe_2O_4$@PGSA core–shell (Fig. 4c). Regarding the Bentonite@$MgFe_2O_4$@PGSA/Cu nanocomposite, the immobilization of copper ion on Bentonite@$MgFe_2O_4$@PGSA does not affect the crystal structure of Bentonite@$MgFe_2O_4$. In this figure, distinct peaks in 2θ = 21.4 and 28.3° regions are indexed to copper metal that overlaps with peaks related to PGSA (Fig. 4d).

The FESEM images of Bentonite@$MgFe_2O_4$ (Fig. 5A and B) revealed the existence of spherical $MgFe_2O_4$ NPs over the bentonite matrix. Notably, the average grain size was 20–35 nm. The FE-SEM image indicates the layered structure of PGSA (Fig. 5C and D). The FE-SEM image of Bentonite@$MgFe_2O_4$@PGSA shows the layered structure of PGSA, as formed on the surface of $MgFe_2O_4$@Bentonite nanocomposite. The presence of PGSA is an essential factor to prevent agglomeration. The figure shows the coexistence of Bentonite@$MgFe_2O_4$ and PGSA on the surface of the prepared catalyst (Fig. 5E). The surface morphology of Bentonite@$MgFe_2O_4$@PGSA/Cu is shown in Fig. 5F. This figure shows the coexistence of Bentonite@$MgFe_2O_4$ and PGSA on the surface of the prepared catalyst. Significantly, the distribution of copper ions on the surface of Bentonite@$MgFe_2O_4$@PGSA did not change the support morphology.

The size distribution of Bentonite@$MgFe_2O_4$@PGSA/Cu MNPs was investigated using transmission electron microscopy (TEM) (Fig. 6A–D). The TEM images of Bentonite@$MgFe_2O_4$@PGSA/Cu MNPs show some specific aggregation (Fig. 6A and B), probably due to the magnetic nature of $MgFe_2O_4$, which indicates that the coatings were not much effective in stopping the aggregation. Overall, these observations confirm the successful coating of PGSA (the bright area) on Bentonite@$MgFe_2O_4$ (*i.e.*, the dark area). Besides, a sharp gap between the support and shell proves the support's spherical solid morphology. Furthermore, a stacking texture with slight aggregation is developed regarding the interparticle magnetic attractions. At the same time, copper loading did not change the support morphology, and the prepared catalyst showed some features of the crystalline structure.

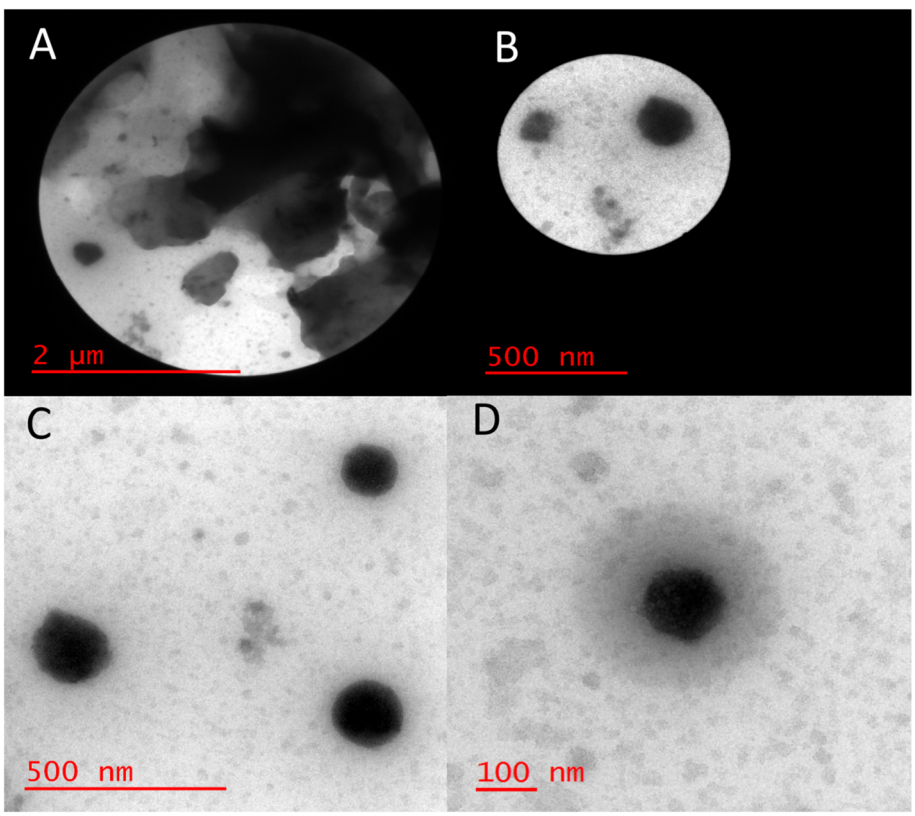

Fig. 6 HRTEM image of Bentonite@$MgFe_2O_4$@PGSA/Cu MNPs at different scale 2μm (A), 500 nm (B and C), 100 nm (D).

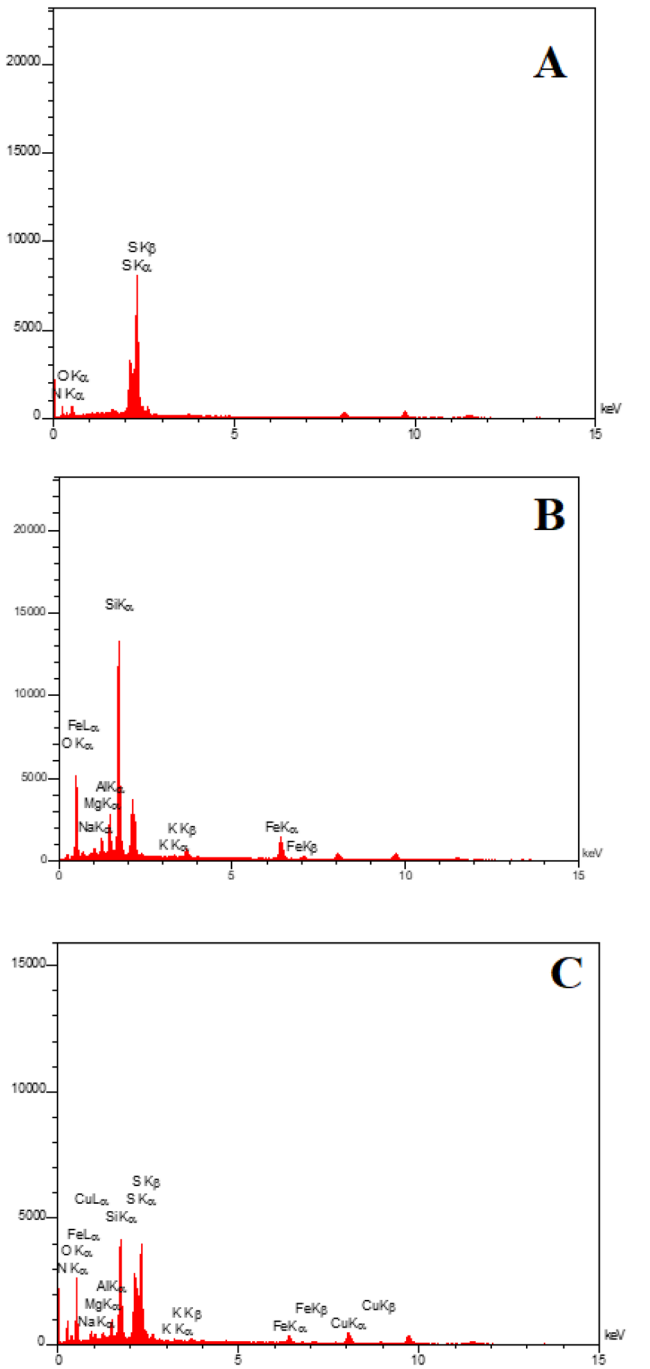

Fig. 7 EDX spectrum of (A) PGSA, (B) Bentonite@$MgFe_2O_4$, (C) Bentonite@$MgFe_2O_4$@PGSA/Cu nanocomposite.

EDAX analysis confirmed the presence of C, N, O, and S elements for PGSA (Fig. 7A) and Fe, O, Mg, and Al for Bentonite@$MgFe_2O_4$ (Fig. 7B). The EDX analysis of Bentonite@$MgFe_2O_4$@PGSA/Cu nanocomposite confirms the presence of all studied elements (Fig. 7C). The elemental mapping study of Bentonite@$MgFe_2O_4$@PGSA/Cu MNPs indicates the uniform distribution of elemental components in the prepared structure (Fig. 8).

Fig. 9 illustrates the ^{1}H NMR spectra of PGSA. The peaks corresponding to the aromatic groups appear in the range of 7.06–7.62 ppm, while the amine peaks appear in the range of 7.96–8.26 ppm.

3.2. Application of Bentonite@$MgFe_2O_4$@PGSA/Cu

As shown in Table 2, *p*-chlorobenzaldehyde, malononitrile, ethyl acetoacetate, and hydrazine hydrate were used as substrates for the optimization study. Initially, based on our observations, in the absence of the catalyst, the reaction could not proceed even after a long reaction time (entry 1). Then, the effect of several solvents, *i.e.*, DMF, toluene, ethanol, and the solvent-free ones, has been also screened. The reaction preceded in toluene with a good yield of the product (68%). Water, the best choice for this reaction, yielded the product at up to 98%. Using DMF and EtOH as the solvent decreased the yield (entries 2–6). This superior catalytic performance of Bentonite@$MgFe_2O_4$@PGSA/Cu in water can be attributed to the amphiphilic behavior of the surface multifunctionalization of Bentonite@$MgFe_2O_4$ using polyguanidinesulfonamide units. The examination of various catalyst loadings (entries 7–8) revealed that 0.1 mol% (entry 5) was optimal for the best catalytic results. Finally, Bentonite@$MgFe_2O_4$@PGSA, Bentonite@$MgFe_2O_4$, and PGSA were investigated to compare their catalytic performance. However, moderate yields are related to the effect of functionalization (entries 9–12).

The generality and scope of the reaction were explored on numerous aldehydes under the optimum conditions, the results of which are given in Table 3. In this sense, the electron-withdrawing groups on aromatic aldehydes yielded the desired alcohols in high yields and high reaction rates (entries 1–5). Although the electron-donating groups also led to high yielded additions, the rates of conversion were higher (entries 6–8). Moreover, this methodology was successfully used for hetero-aromatic benzaldehydes such as thiophene-2-carbaldehyde, furfural, and isonicotinaldehyde (entries 9–11), producing the corresponding product in excellent yield without forming any byproduct. Furthermore, reactions with 2-naphthaldehyde and [1,1′-biphenyl]-4-carbaldehyde afforded the corresponding products in high yields (entries 12–13).

3.3. Investigation of the mechanism of the reaction

The Knoevenagel reaction has been successfully employed as a starting point for many multicomponent reactions. At the beginning of the reaction, Bentonite@$MgFe_2O_4$@PGSA/Cu activates the carbonyl groups in the 1,3-dicarbonyl compound and then hydrazine hydrate attacks the activated carbonyl groups to generate pyrazolone (I), which was further rearranged into tautomer (II) *via* keto–enol tautomerization. Afterward, the Bentonite@ $MgFe_2O_4$@PGSA/Cu Lewis acid catalyzed the Knoevenagel condensation of aryl aldehydes with active methylene compound (malononitrile), followed by the elimination of a water molecule to produce an α,β-unsaturated intermediate (III). Subsequently, Michael 1,4-addition (or conjugate addition) reaction between tautomer (II) and the activated intermediate (III) is facilitated to form intermediate

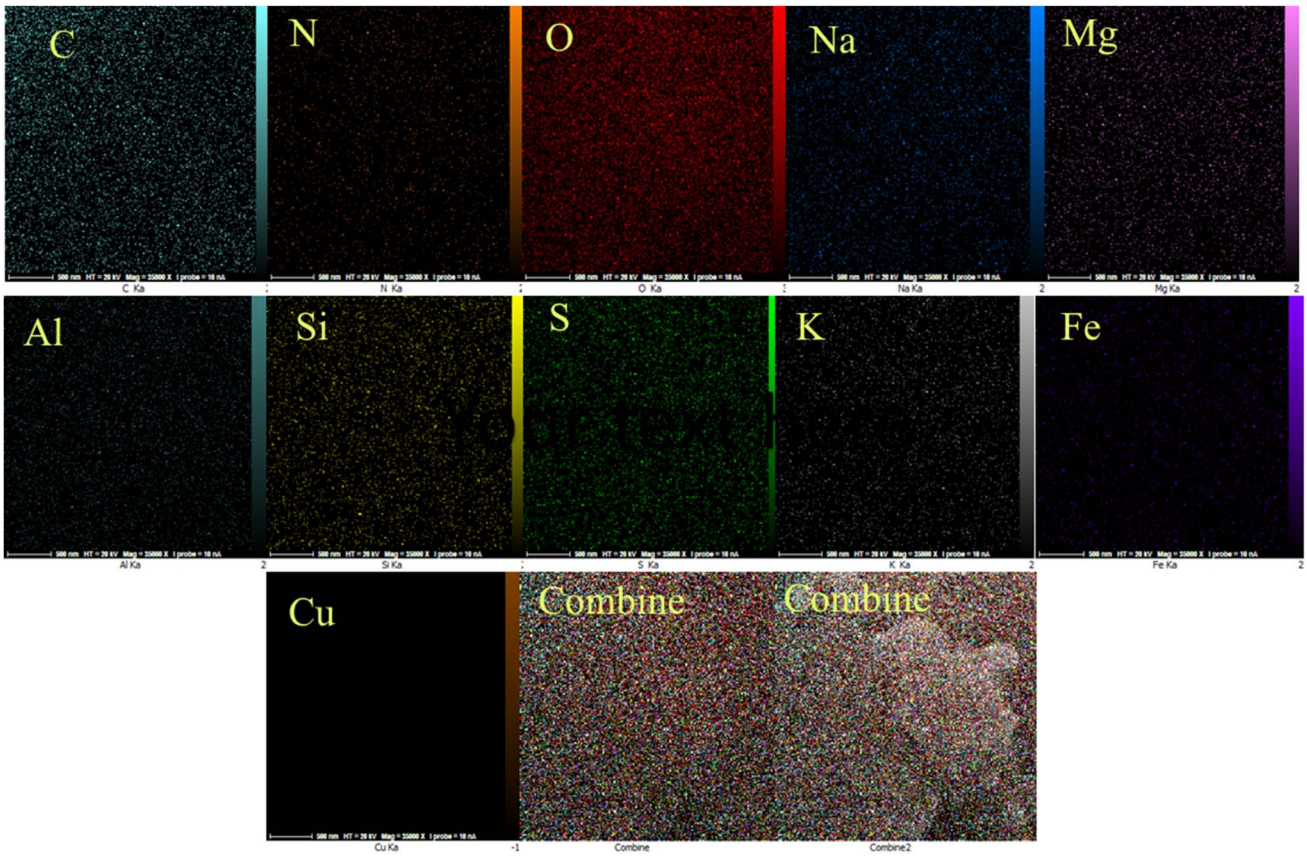

Fig. 8 Elemental mapping of the atoms achieved from the SEM micrographs.

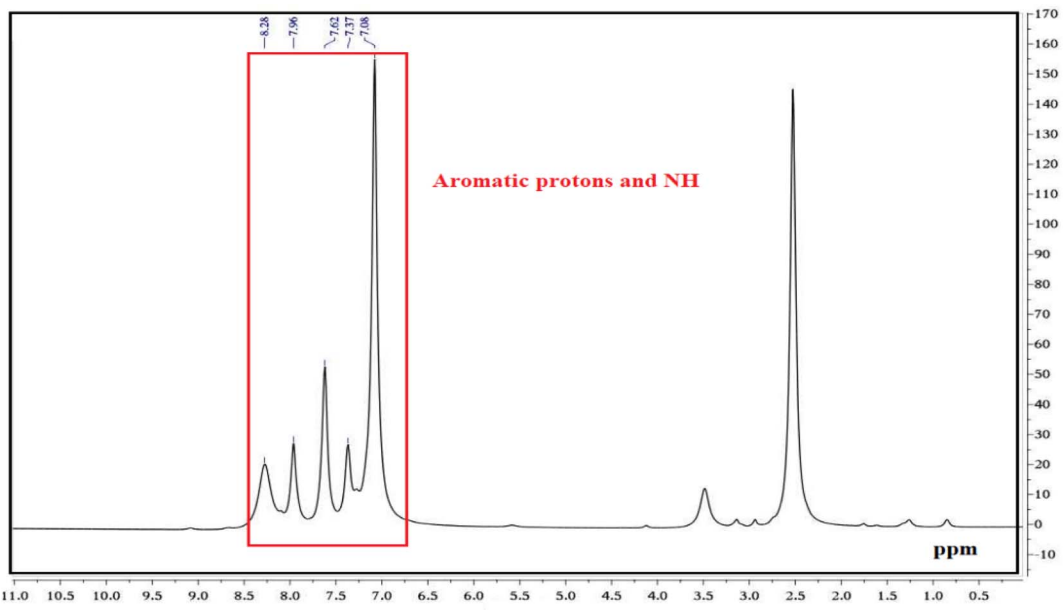

Fig. 9 HNMR of PGSA.

(IV), which undergoes an intramolecular cyclization reaction. Finally, the target products are formed *via* tautomerization (1,3 H shift)[48,49] (Scheme 3).

The recovery and reusability of the nanomagnetic catalysts were completed to examine the stability and preservation of the catalytic activity. The reaction was done in the presence of the

Table 2 Optimization of reaction conditions

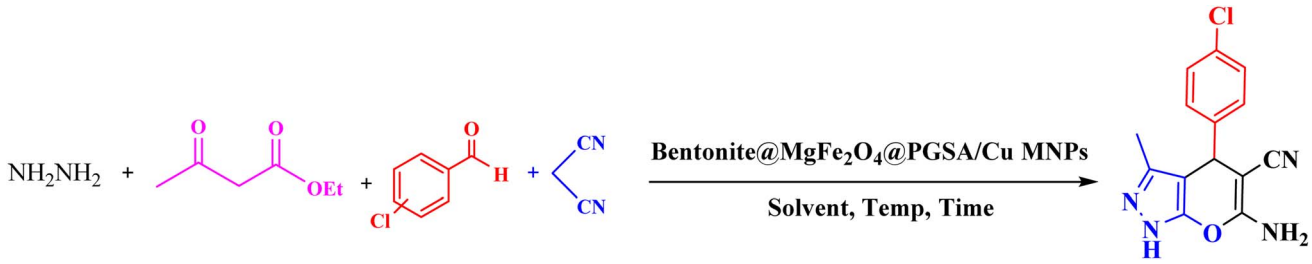

Entry	Cat. (mol%)	Solvent	Time (min)	Yield[a] (%)
1	—	H_2O	30	N.R.
2	Bentonite@$MgFe_2O_4$@PGSA/Cu (0.2)	DMF	30	80
3	Bentonite@$MgFe_2O_4$@PGSA/Cu (0.2)	Toluene	60	68
4	Bentonite@$MgFe_2O_4$@PGSA/Cu (0.2)	EtOH	15	90
5	Bentonite@$MgFe_2O_4$@PGSA/Cu (0.2)	Solvent-free	30	72
6	Bentonite@$MgFe_2O_4$@PGSA/Cu (0.2)	H_2O	10	98
7	Bentonite@$MgFe_2O_4$@PGSA/Cu (0.1)	H_2O	10	73
8	Bentonite@$MgFe_2O_4$@PGSA/Cu (0.3)	H_2O	10	96
9[b]	Bentonite@$MgFe_2O_4$ (0.05 g)	H_2O	30	65
10[c]	PGSA (0.05 g)	H_2O	30	55
11[d]	Bentonite@$MgFe_2O_4$ @PGSA (0.05 g)	H_2O	20	83
12[e]	Bentonite@$MgFe_2O_4$/Cu (0.2)	H_2O	30	75

[a] Isolated yield. [b] The model reaction was examined in the presence of Bentonite@$MgFe_2O_4$. [c] The model reaction was examined in the presence of PGSA. [d] The model reaction was examined in the presence of Bentonite@$MgFe_2O_4$ @PGSA. [e] The model reaction was examined in the presence of Bentonite@$MgFe_2O_4$/Cu.

Table 3 Synthesis of pyrano[2,3-c]pyrazoles from different aldehydes using Bentonite@$MgFe_2O_4$ @PGSA/Cu[a]

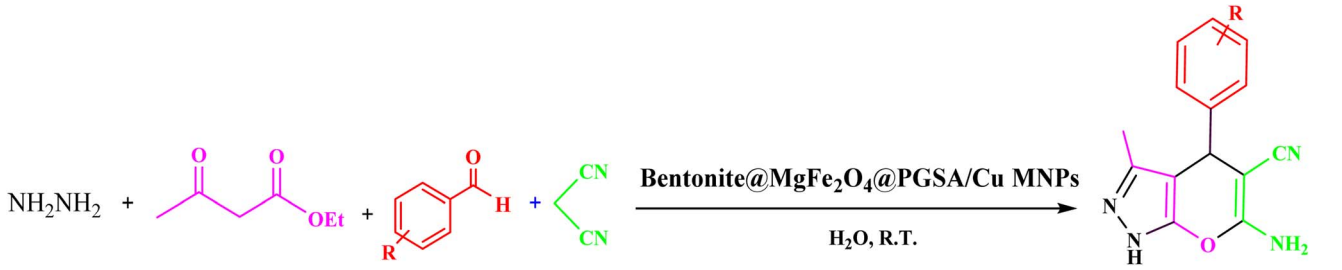

Entry	Substrate	Product	Time (min)	Yield[b] (%)	Melting point (°C) Measured	Melting point (°C) Literature
1	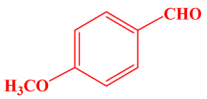	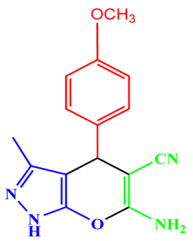 **5a**	20	90	262–264	262–264 (ref. 42)
2	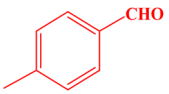	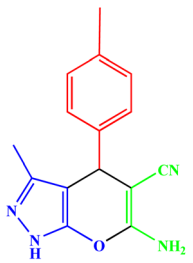 **5b**	20	92	82–83	82–83 (ref. 42)
3	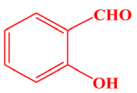	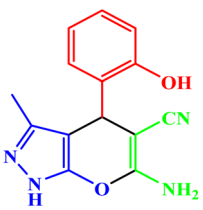 **5c**	25	90	247–249	247–249 (ref. 43)
4		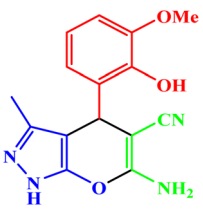 **5d**	20	94	240–242	240–242 (ref. 43)

Table 3 (*Contd.*)

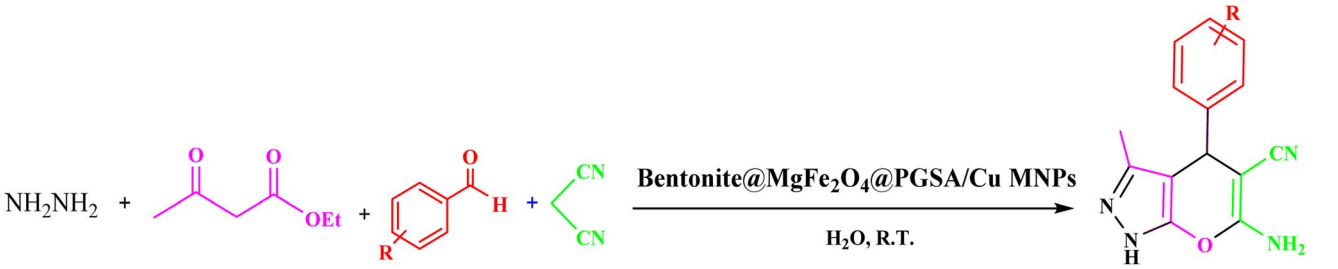

Entry	Substrate	Product	Time (min)	Yield[b] (%)	Melting point (°C) Measured	Melting point (°C) Literature
5	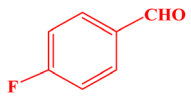	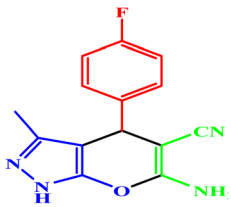 **5e**	15	95	97–98	95–97 (ref. 43)
6	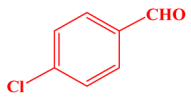	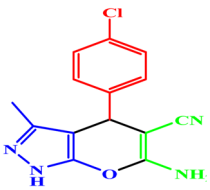 **5f**	10	98	243–245	244–245 (ref. 43)
7	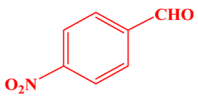	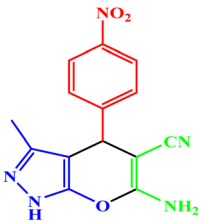 **5g**	10	95	244–246	244–246 (ref. 43)
8	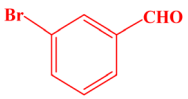	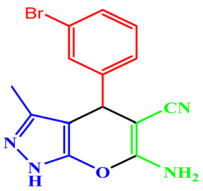 **5h**	10	98	258–260	259–261 (ref. 43)
9	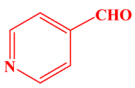	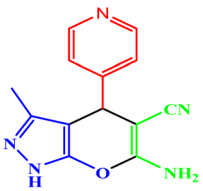 **5i**	10	91	69–70	69–70 (ref. 42)

Table 3 (*Contd.*)

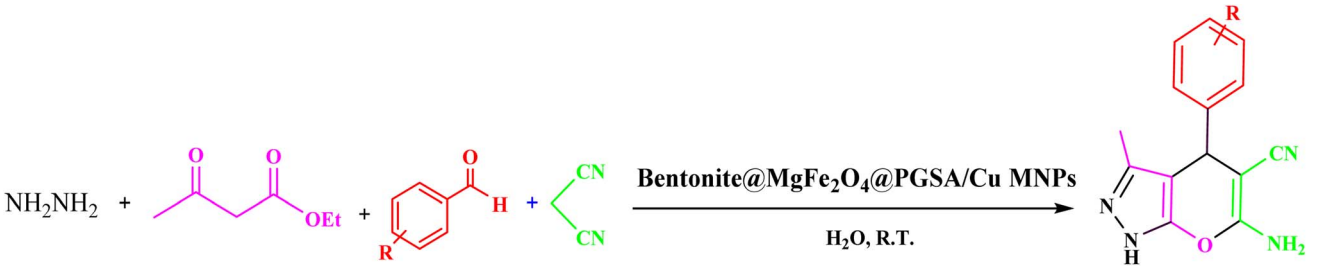

Entry	Substrate	Product	Time (min)	Yield[b] (%)	Melting point (°C) Measured	Melting point (°C) Literature
10	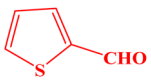	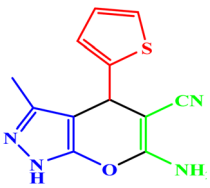 **5j**	10	95	211–212	212–213 (ref. 42)
11	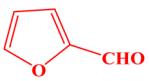	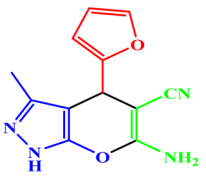 **5k**	10	94	241–243	240–242 (ref. 42)
12	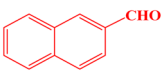	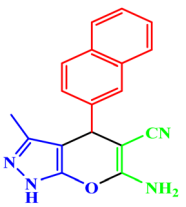 **5l**	15	93	224–226	226–228 (ref. 43)
13	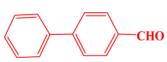	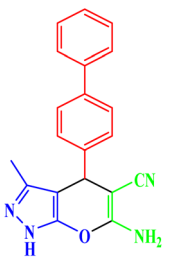 **5m**	15	88	220–221	224–225 (ref. 43)

[a] Reaction conditions: benzaldehyde derivatives (1 mmol), ethyl acetoacetate (1 mmol), hydrazine hydrate (1 mmol), malononitrile (1 mmol); and Bentonite@$MgFe_2O_4$@PGSA/Cu (0.2 mol%) were stirred at room temperature. [b] Isolated yield.

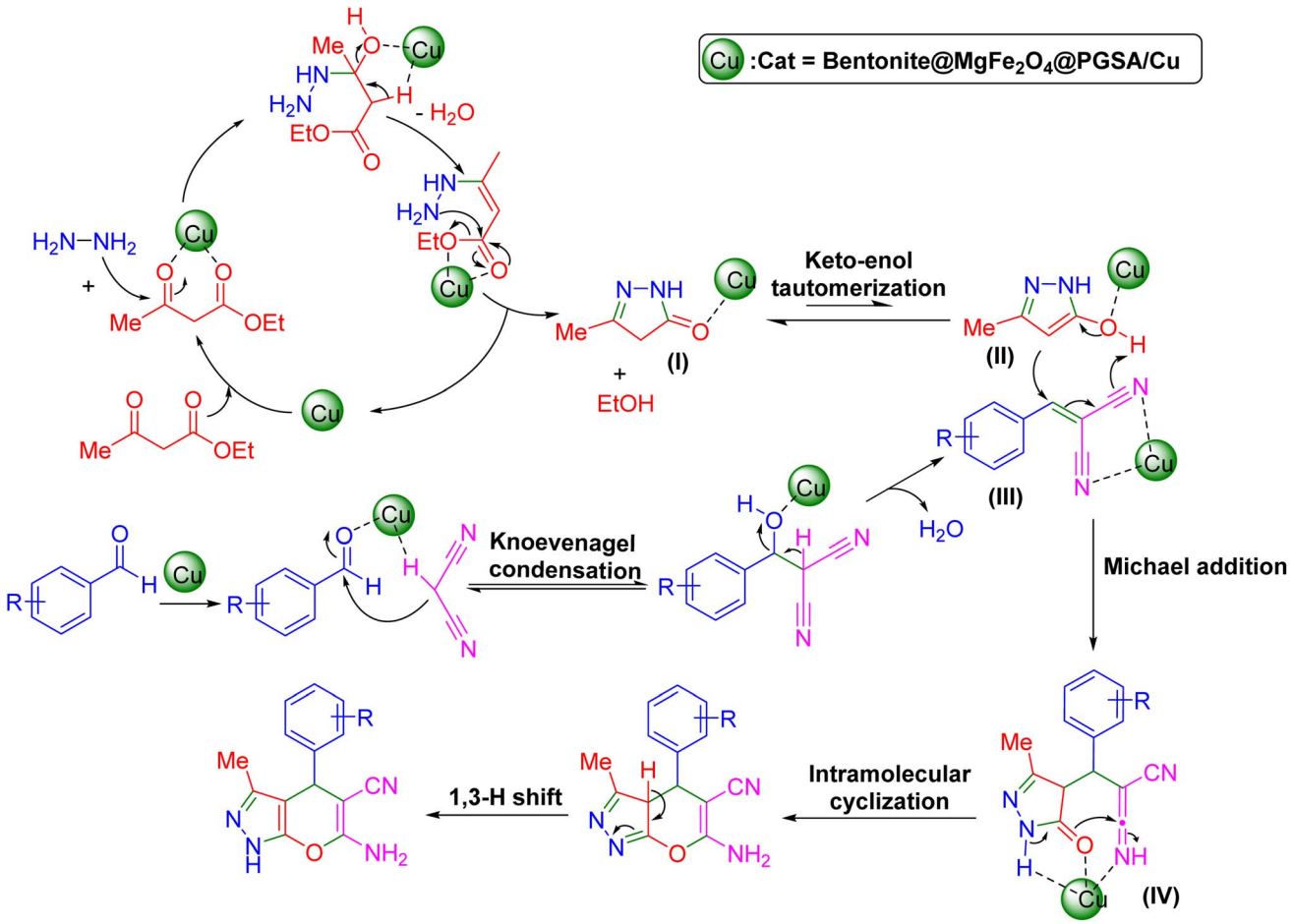

Scheme 3 The plausible reaction mechanism of Bentonite@$MgFe_2O_4$@PGSA/Cu-catalyzed synthesis of pyrano[2,3-c]pyrazoles.

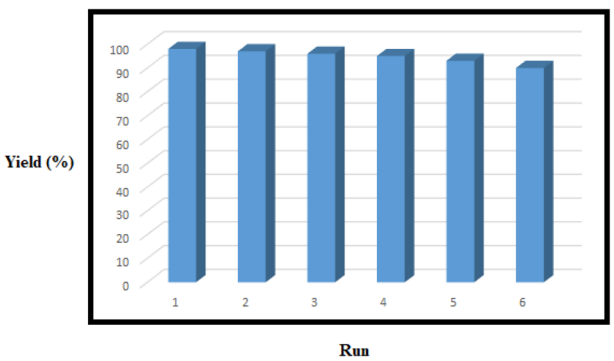

Fig. 10 Recycling of the Bentonite@$MgFe_2O_4$@PGSA/Cu for the reaction of benzaldehyde, ethyl acetoacetate, hydrazine hydrate, and malononitrile.

six-time recycled Bentonite@$MgFe_2O_4$@PGSA/Cu without a notable decrease in the activity (Fig. 10). The negligible decrease is due to the catalyst loss during the recycling procedure (the concentration of silver was determined by ICP-AES that changed 1.3% to 1.28% after the 6th run). Therefore, the Bentonite@$MgFe_2O_4$@PGSA/Cu are highly stable under the studied reaction conditions.

4 Conclusion

In conclusion, the current study found a path to change bentonite to a worthy solid catalyst. The immobilization of copper ion on core–shell Bentonite@$MgFe_2O_4$@PGSA gives a heterogeneous, green, and recyclable solid acid catalyst for the synthesis of 1,4-dihydropyrano[2,3-*c*] pyrazole compounds. Furthermore, the prevailing synthesis technique is a type of green, powerful, easy, economical, and environmental strategy to prepare other composites with bentonite and other clay as the support. As a result, bentonite was transformed into a magnetic, green, cheap, and environment-friendly catalyst. The highlights of this work were the mild reaction conditions, the retrievability of the nanocomposite for at least six times, high yields, and environment-friendly profiles with the traditional protocols.

Conflicts of interest

The authors declare no competing interests.

Acknowledgements

The authors thank Bu-Ali Sina University, Center of Excellence Developmental of Environmentally Friendly Methods for

Chemical Synthesis (CEDEFMCS), and the Iran National Science Foundation (INSF) for financial support to carry out this research.

References

1 G. A. Coppola, S. Pillitteri, E. V Van der Eycken, S.-L. You and U. K. Sharma, *Chem. Soc. Rev.*, 2022, **51**, 2313–2382.
2 L. Levi and T. J. J. Müller, *Chem. Soc. Rev.*, 2016, **45**, 2825–2846.
3 M. Kazemi and M. Mohammadi, *Appl. Organomet. Chem.*, 2020, **34**, e5400.
4 M. Mohammadi and A. Ghorbani-Choghamarani, *RSC Adv.*, 2022, **12**, 26023–26041.
5 A. Shabanloo, R. Ghorbani-Vaghei and S. Alavinia, *Org. Prep. Proced. Int.*, 2020, 402–409.
6 R. Ghorbani-Vaghei, S. Alavinia and N. Sarmast, *Appl. Organomet. Chem.*, 2018, **32**, e4038.
7 C. Wang, B. Yu, W. Li, W. Zou, H. Cong and Y. Shen, *Mater. Today Chem.*, 2022, **25**, 100948.
8 D. Becerra, R. Abonia and J.-C. Castillo, *Molecules*, 2022, **27**, 4723.
9 J. Babamoradi, S. Alavinia, R. Ghorbani-Vaghei and R. Azadbakht, *New J. Chem.*, 2022, **46**, 23394–23403.
10 T. Tamoradi, S. M. Mousavi and M. Mohammadi, *New J. Chem.*, 2020, **44**, 3012–3020.
11 M. T. Nazeri, T. Nasiriani, H. Farhid, S. Javanbakht, F. Bahri, M. Shadi and A. Shaabani, *ACS Sustainable Chem. Eng.*, 2022, **10**, 8115–8134.
12 L. Botta, S. Cesarini, C. Zippilli, B. M. Bizzarri, A. Fanelli and R. Saladino, *Curr. Med. Chem.*, 2022, **29**, 2013–2050.
13 S. Pasricha, K. Mittal, P. Gahlot, H. Kaur, N. Avasthi and S. Bisht, *J. Iran. Chem. Soc.*, 2022, **19**, 4035–4092.
14 S. Solgi, R. Ghorbani-Vaghei, S. Alavinia and V. Izadkhah, *Polycyclic Aromat. Compd.*, 2022, **42**, 2410–2419.
15 D. Dwarakanath and S. L. Gaonkar, *Asian J. Org. Chem.*, 2022, **11**, e202200282.
16 F. Hassanzadeh-Afruzi, Z. Amiri-Khamakani, S. Bahrami, M. R. Ahghari and A. Maleki, *Sci. Rep.*, 2022, **12**, 4503.
17 H. Kiyani and M. Bamdad, *Res. Chem. Intermed.*, 2018, **44**, 2761–2778.
18 F. Mohamadpour, *J. Chem. Sci.*, 2020, **132**, 72.
19 L. Chiummiento, R. D'Orsi, M. Funicello and P. Lupattelli, *Molecules*, 2020, **25**, 2327.
20 H. R. Shaterian and M. Kangani, *Res. Chem. Intermed.*, 2014, **40**, 1997–2005.
21 M. A. Shaikh, M. Farooqui and S. Abed, *Res. Chem. Intermed.*, 2019, **45**, 1595–1617.
22 M. Beerappa and K. Shivashankar, *Synth. Commun.*, 2018, **48**, 146–154.
23 H. Kashtoh, M. T. Muhammad, J. J. A. Khan, S. Rasheed, A. Khan, S. Perveen, K. Javaid, W. Atia tul, K. M. Khan and M. I. Choudhary, *Bioorg. Chem.*, 2016, **65**, 61–72.
24 J. Safaei-Ghomi, A. Ziarati and M. Tamimi, *Acta Chim. Slov.*, 2013, **60**, 403–410.
25 H. Faroughi Niya, N. Hazeri and M. T. Maghsoodlou, *Appl. Organomet. Chem.*, 2020, **34**, e5472.
26 R. Ghiai, S. Alavinia, R. Ghorbani-Vaghei and A. Gharakhani, *RSC Adv.*, 2022, **12**, 34425–34437.
27 Z. Zhuang and D. Liu, *Nano-Micro Lett.*, 2020, **12**, 132.
28 A. Tombesi and C. Pettinari, *Inorganics*, 2021, **9**, 81.
29 R. Zhang, Y. Chen, M. Ding and J. Zhao, *Nano Res.*, 2022, **15**, 2810–2833.
30 S. Alavinia and R. Ghorbani-Vaghei, *J. Mol. Struct.*, 2022, **1270**, 133860.
31 S. Alavinia, R. Ghorbani-Vaghei, S. Asadabadi and A. Atrian, *Mater. Chem. Phys.*, 2023, **293**, 126915.
32 M. Jiang, R. Dong, H. Liao, Y. Liu, Y. Wang, P. Tan and J. Pan, *Electrochim. Acta*, 2022, **425**, 140665.
33 A. Benali, L. Saher, M. Bejar, E. Dhahri, M. F. P. Graca, M. A. Valente, P. Sanguino, L. A. Helguero, K. Bachari, A. M. S. Silva and B. F. O. Costa, *Eur. Phys. J. Plus*, 2022, **137**, 559.
34 M. Mohammadi and A. Ghorbani-Choghamarani, *Appl. Organomet. Chem.*, 2022, **36**, e6905.
35 V. Izadkhah, R. Ghorbani-Vaghei, S. Alavinia, S. Asadabadi, N. Emami and S. Jamehbozorgi, *J. Mol. Struct.*, 2023, **1275**, 134691.
36 M. A. Zolfigol, D. Habibi and B. B. F. Mirjalili, *Tetrahedron Lett.*, 2003, **44**, 3345–3349.
37 M. K. Bharti, S. Chalia, P. Thakur, S. N. Sridhara, A. Thakur and P. B. Sharma, *Environ. Chem. Lett.*, 2021, **19**, 3727–3746.
38 J. Y. Shen, J. J. Mo, Y. C. Tao, Y. F. Xia and M. Liu, *J. Low Temp. Phys.*, 2022, **209**, 166–181.
39 W. Xue, D. Huang, X. Wen, S. Chen, M. Cheng, R. Deng, B. Li, Y. Yang and X. Liu, *J. Hazard. Mater.*, 2020, **390**, 122128.
40 D. K. Jambhulkar, R. P. Ugwekar, B. A. Bhanvase and D. P. Barai, *Chem. Eng. Commun.*, 2022, **209**, 433–484.
41 R. Ramesh, V. Tamilselvi, P. Vadivel and A. Lalitha, *Polycyclic Aromat. Compd.*, 2020, **40**, 811–823.
42 N. Thomas, D. D. Dionysiou and S. C. Pillai, *J. Hazard. Mater.*, 2021, **404**, 124082.
43 A. Ahmadi, R. Foroutan, H. Esmaeili, S. J. Peighambardoust, S. Hemmati and B. Ramavandi, *Mater. Chem. Phys.*, 2022, **284**, 126088.
44 C. Guo, F. Cheng, G. Liang, S. Zhang, Q. Jia, L. He, S. Duan, Y. Fu, Z. Zhang and M. Du, *Chem. Eng. J.*, 2022, **435**, 134915.
45 S. Alavinia and R. Ghorbani-Vaghei, *J. Phys. Chem. Solids*, 2020, **146**, 109573.
46 S. Alavinia, R. Ghorbani-Vaghei, J. Rakhtshah, J. Yousefi Seyf and I. Ali Arabian, *Appl. Organomet. Chem.*, 2020, **34**, e5449.
47 L. Zhu, H. Huang, Y. Wang, Z. Zhang and N. Hadjichristidis, *Macromolecules*, 2021, **54**, 8164–8172.
48 M. Koolivand, M. Nikoorazm, A. Ghorbani-Choghamarani and M. Mohammadi, *Appl. Organomet. Chem.*, 2022, **36**, e6656.
49 H. T. Nguyen, T. V. Le and P. H. Tran, *J. Environ. Chem. Eng.*, 2021, **9**, 105228–110523.